



NEUTRONIC ANALYSIS OF THE DEN-R1 SUBCRITICAL NUCLEAR REACTOR

,

¹ UFMG, Av. Pres. Antônio Carlos, 6627, Escola de Engenharia, Bloco 4, DEN
Pampulha, Belo Horizonte - MG, 31270-901

Keywords: Neutronic Analysis, OpenMC, Subcritical Nuclear Reactor, NC-9000

ABSTRACT

DEN-R1 is a thermal subcritical nuclear research reactor, manufactured by Nuclear Chicago Corporation, USA, model NC-9000. It is a tank-type reactor fueled by uranium, moderated and reflected by water, with a single fuel element consisting of 283 rods arranged in a hexagonal matrix. The central rod contains water and is the place to insert a neutron source, while the remaining 282 rods are filled with air, each housing five compacted natural uranium ring bars stacked vertically, also coated with aluminum. This study aims to conduct a comprehensive neutronic analysis of the reactor, focusing on the multiplication factor, subcritical multiplication, neutron amplification factor, neutron flux energy spectrum, spatial flux distribution, and identification of optimized irradiation spots for sample insertion. The article provides a detailed description of the materials used and the reactor's geometric configuration. Simulation results, obtained using the OpenMC Monte Carlo code, include calculations of the multiplication factor, fission rate, neutron flux distribution and energy spectrum.

1. INTRODUCTION

In the 1960s, ITA (Technological Institute of Aeronautics, in portuguese Instituto Tecnológico de Aeronáutica) inaugurated a subcritical nuclear reactor of model NC-9000 (Nuclear Chicago 9000) manufactured by Nuclear Chicago Corporation, from U.S.A. Later, it was donated to UFMG (Federal University of Minas Gerais, in portuguese Universidade Federal de Minas Gerais) in the 1990's, where become DEN-R1. The parts of the reactor, shown in Fig. 1, comprise a tank-type subcritical reactor moderated and reflected by light water, fueled with natural uranium.

The reactor core has a single fuel element composed of 283 rods arranged in a hexagonal matrix, with an additional 30 positions available for rods of any material in the peripheral regions of the reactor core, allowing for the rearrangement of rods as needed. The central tube is filled with water and contain space for the neutron source allocation and for sample irradiation.

Remaining rods are filled with air, each housing five cylindrical annular bars of compacted natural uranium, coated with aluminium, arranged one above the other. Fuel rods are under safeguard system of CNEN (National Nuclear Energy Commission, in portuguese Comissão Nacional de Energia Nuclear), pending commissioning of nuclear installation at DEN/UFMG (Departament of Nuclear Engineering at UFMG).

The model NC-9000 is designed with nuclear and radiological safety in mind, allowing users, including students and faculty, to perform tasks such as inserting or removing detectors, irradiating samples, handling fuel rods, and conducting measurements [2].

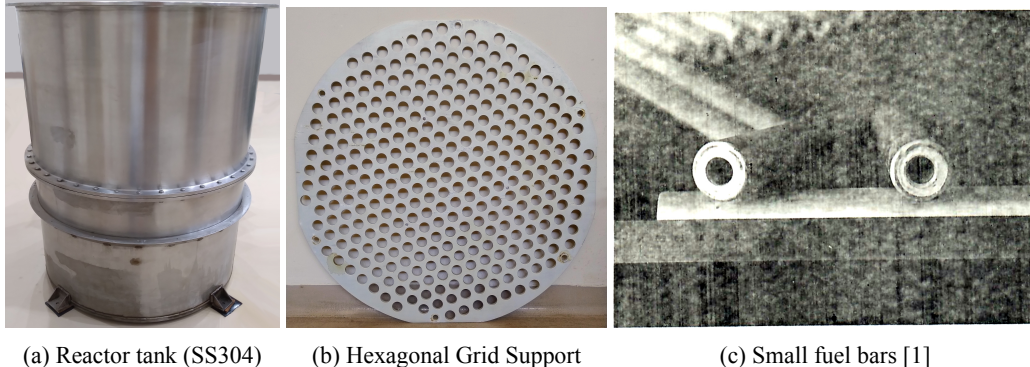


Figure 1. Photos of reactor components.

A master's dissertation from ITA [1] analyzed the characteristics of this reactor, where it was found that some data provided by the manufacturer were incorrect. For example, the manufacturer provided the pitch measurement (distance between the centers of two closest bars) as 1.75 in, while measuring the hexagonal grid (Fig. 1b) it was found that it is actually 2 in. Since geometry has changed, it would generate differences in effective multiplication factor compared to that provided by manufacturer.

Under these circumstances, it is important for DEN to conduct a neutronic study of the reactor prior to its installation. The aim of this work is to calculate the effective multiplication factor, subcritical multiplication factor, source factor and neutron multiplication. After that, the Neutron flux is mapped throughout the reactor, considering two energy groups: thermal and fast. Then, the neutron flux is assessed in the irradiation regions positions, considering these thermal and fast energy groups and the neutron flux spectrum that these irradiation regions.

2. METHODOLOGY

To simulate DEN-R1, it is essential that the geometry model and material compositions are aligned with the reference data. Simulation settings should be comprehensively detailed, including the source of input data and the uncertainty margins associated with the results.

2.1. Geometry and Materials

The fuel consists of a annular bar of compacted natural uranium, encased in a 1 mm aluminium layer on sides and 5 mm on top and bottom. Each fuel rod is composed of five small bars, totaling 282 fuel rods. These bars weight about 1867 g each, representing a total of 2630 kg of natural compacted uranium. To calculate this mass, Motta [1] determined the density using gamma radiography, revealing that the manufacturer's reported density of 18.7 g cm^{-3} was higher, while the measured value was 18.0 g cm^{-3} . The fuel has an external diameter of 3.07 cm, an internal diameter of 1.27 cm, and a length of 21.45 cm, as depicted in Fig. 2b.

Light water is used as moderator, coolant, and reflector, requiring deionization resin treatment to remove dissolved ions. Two types of resins are employed: cationic resins to remove cations and anionic resins to remove anions. The water level is maintained at 135 cm to ensure is above the fuel. As shown in Fig. 2, there is no reflector material at the top of the reactor; however, there is 16.5 cm of water at the bottom and 20 cm at the sides.

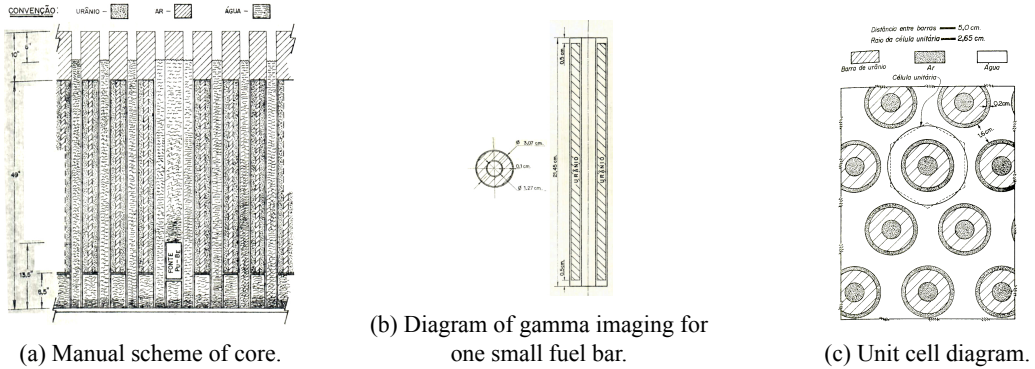


Figure 2. Geometric configuration according to Motta [1]

Fuel rods are arranged in a hexagonal grid with a pitch distance of 5.08 cm, and the entire core is housed in a cylindrical vessel with a height of 150 cm and a diameter of 122 cm made of stainless steel and has a thickness of 1.2 cm. Furthermore, the upper hexagonal grid is positioned 28.4 cm above the vessel's bottom, while the lower grid is fixed at the bottom with a space of 2.54 cm. This reactor model was developed in *OpenMC 0.15.0* [3], as shown in Fig. 3.

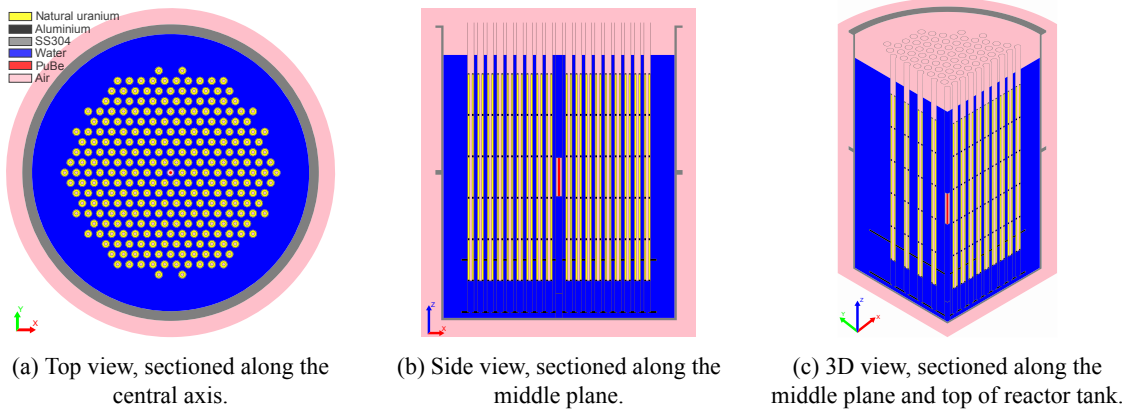


Figure 3. Geometric configuration modelled in *OpenMC*.

It is worth to note that the source of neutrons is positioned at the center of the fuel, and the nuclear data library for photons and neutrons used in this work is *ENDF/B-VIII.0*. As this is a zero-power reactor designed for research purposes, the fuel temperature and all other materials are set to ambient temperature, specifically 294 K. All necessary data to build this model, except for the source materials, are derived from the references Motta [1], KAERI [4], and Huang, Zhang, Dai, *et al.* [5].

2.2. Neutron Source

Three $^{239}\text{PuBe}$ neutron source was used in this reactor on ITA, as described by Motta [1]. These sources were provided by the Nuclear Material and Equipment Corporation in Pennsylvania. They contain 80 g of plutonium and have a total activity of 0.185 TBq. The sources are housed in cylindrical stainless steel containers, which are secured inside an aluminum tube with a diameter of



3 cm and a length of 20 cm. Their neutron yields are 1.87×10^6 , 3.53×10^6 , and $3.86 \times 10^6 \text{ s}^{-1}$, totaling a source strength of $9.26 \times 10^6 \text{ s}^{-1}$. This work uses a very similar $^{239}\text{PuBe}$ source described by Vega-Carrillo, Hernández-Dávila, Rivera, *et al.* [6].

This source contains approximately 80 g of plutonium and 40 g of beryllium, with a ^{239}Pu isotopic fraction of 0.9301. Considering isotopic fractions of 0.0676 and 0.0023 for ^{240}Pu and ^{241}Pu , respectively, the source density is approximately 4.6781 g cm^{-3} . Manufactured by Monsanto Research Corporation on June 22, 1967, the source initially had a nominal ^{239}Pu activity of 0.185 TBq and a neutron yield of $9.04 \times 10^6 \text{ s}^{-1}$. Over time, the reduction in neutron yield due to ^{239}Pu decay has been offset by the increased yield from rising ^{241}Pu impurities. As a result, after 44 years, the source has a neutron yield of $1.01 \times 10^7 \text{ s}^{-1}$. The emission spectrum of the source is discretized into nine distinct energy levels: 3.7×10^4 , 7.8×10^4 , 1.7×10^5 , 3.1×10^5 , 7.0×10^5 , 1.0×10^6 , 2.9×10^6 , 5.6×10^6 and $1 \times 10^7 \text{ eV}$, with corresponding emission probabilities of 0.115, 0.289, 0.641, 1.48, 7.05, 10.9, 14.8, 26.9 and 37.8 %, respectively.

2.3. Simulation Settings

To simulate with accuracy, an *OpenMC* cluster compiled with *OpenMP* and *OpenMPI* was developed. It was composed by 6 processors, totaling 80 cores and 160 threads, distributed across 4 servers.

With this computational power, it was possible to perform in a timely manner fixed source simulations with 100 cycles and 1×10^7 particles, and eigenvalue simulations with 1000 active cycles, 200 skipping cycles and also 1×10^7 particles.

2.4. Analysis and Uncertainty Quantification

Uncertainties are kept below a margin of 5 % for all tallies obtained. Except for the subcritical multiplication factor and neutron multiplication factor, error propagation does not need to be calculated due to the straightforward normalization of results, which considers only the source strength and the volume of the meshes.

2.4.1. Neutronic Parameters

It is important to determine some key neutronic parameters for subcritical systems: multiplication factor (k_{eff}), subcritical multiplication factor (k_s), neutron amplification factor (M) and the importance of external neutron source (ϕ^*). The parameter k_s represents the fraction of neutrons generated by fission relative to the total neutron population. So, it depends of both: the subcritical reactor system and the external source. And its directly related to M , which is the ratio of total source to fixed source. These parameters are calculated using numerical methods, as shown in Eq. (2.1) [7].

$$k_s = \frac{F}{F + S}; \quad M = \frac{1}{1 - k_s}; \quad \phi^* = \frac{1 - \frac{1}{k_{eff}}}{1 - \frac{1}{k_s}}, \quad (2.1)$$

where F represents the neutrons generated by fission, S represents the neutrons originating from the source.

2.4.2. Spacial and spectrum flux distribution

All the spatial fluxes were divided into 2 energy ranges, namely:

- Thermal range: from $1 \times 10^{-5} \text{ eV}$ to 1.0 eV ;



- Fast range: from 1.0 eV to $1.1 \times 10^7 \text{ eV}$.

Considering the cylindrical geometry of the reactor core, radial and axial meshes were created for neutron counting. For the radial flux, a rectilinear mesh divided into 284^2 parts in 2 directions (X and Y) was used to allow a 2D visualization of flux intensity, in addition to a narrow rectangular mesh divided into 1000 parts in 1 direction (X) for a more detailed visualization of flux variation along the different parts of the reactor. Fig. 4a and Fig. 4b show the position and geometry of rectilinear meshes on cross-sectional views of reactor.

For the axial flux, two axial meshes were created in two different positions: a cylindrical mesh divided into 1000 parts on \vec{Z} direction inside the central rod, and another mesh inside one of six fuel rod closest to central rod, divided the same amount of parts and same direction. The axial meshes were positioned in these locations also considering the possibility of their use for sample irradiation, as they are theoretically locations with the highest flux intensity as they are closer to the center of the reactor and the neutron source at the same time. This statement is verified by tally results corresponding to the previously described regions. Fig. 4a and Fig. 4b also show the position and geometry of axial meshes on cross-sectional views of reactor.

Considering that the highest flux positions within central and fuel rods are closest to the center and source, two meshes were created in available irradiation regions with high flux to investigate the spectrum a sample would be subjected to:

- (1) Positioned above source, inside central tube, arbitrated 1 cm hight; and
- (2) Positioned inside the fuel, internal diameter of the fuel, same size and \vec{Z} position as the source.

Fig. 4c show the position and geometry of axial meshes on cross-sectional views of reactor. The spectrum are divided on 150 energy intervals, from 1×10^{-5} to $1 \times 10^7 \text{ eV}$.

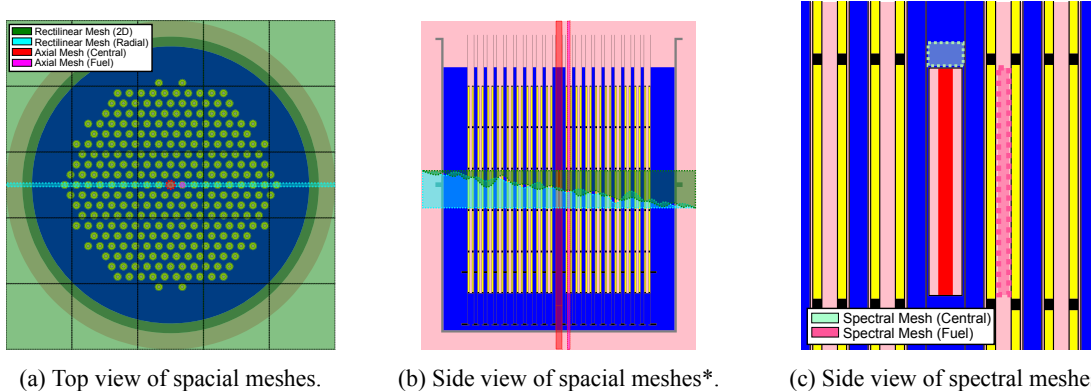


Figure 4. Geometric configuration of meshes in *OpenMC*.

*Blue and green regions overlap because they have same size on \vec{X} and \vec{Z} directions.

3. RESULTS

3.1. Neutronic Behavior and Multiplication Factors Analysis

Tab. 1 compares the value of k_{eff} obtained from simulation (Simu.) performed in this work with values of reference data: Provided by Manufacturer (Manu.) according to Motta [1]; Experiments



(Exp.) performed by Motta [1]; Calculations (Calc.) performed by Motta [1]; and Simulation performed by Vega-Carrillo, Garcia-Reyna, Marquez-Mata, *et al.* [8].

Table 1. Comparison of k_{eff} from simulation performed in this work with other sources.

Source	Simu.	Manu. [1]	Exp. [1]	Calc. [1]	Simu. [8]
k_{eff} mean value	0.841 897	0.842	0.96	0.91	0.8296
Uncertainty	9×10^{-6}	—	—	7×10^{-2}	6×10^{-4}

Simulated k_{eff} closely aligns with manufacturer data, differing by only $1.22 \times 10^{-4}\%$. The calculation from Motta [1] shows a larger difference of 7.5% compared to this work, with a significant margin of error, potentially reaching a lower value of 0.84. Experimentally, this estimate goes even higher reaching a k_{eff} of 0.96.

A similar simulation done by Vega-Carrillo, Garcia-Reyna, Marquez-Mata, *et al.* [8], shows a slightly lower k_{eff} than the obtained in this work, showing a difference of 1.46%. It was also based on 282 fuel rods, but presents a lower density of compacted natural uranium, reported as 14.01 g cm^{-3} , while the fuel simulated in this work has a density of 18 g cm^{-3} , which justifies the difference in the k_{eff} value obtained in both simulations.

As depicted in Tab. 2, the mean value of k_s is higher than k_{eff} , indicating a conservative estimate for cases where the external source is inside the system. The significant contribution of the source to the neutron population is indicated from $\phi^* > 1$, implying that one external source neutron corresponds to 1.87 fission neutrons [7]. In a steady-state subcritical system approaching criticality, the neutron flux distribution becomes similar to that of a critical system with external sources included. Consequently, the value of k_s tends to approximate of k_{eff} , which is not the case here. Finally, the mean value of M indicates a net neutron increase of approximately $11 \times$ the total neutrons emitted by the source.

Table 2. Subcritical multiplication factor of DEN-R1 and related parameters.

Parameters	k_s	ϕ^*	M
Mean value	0.908850	1.872485	10.970965
Uncertainty	1.58×10^{-4}	2.83×10^{-5}	1.90×10^{-2}

The neutron flux distribution, shown in Figs. 5a and 5c, is divided into thermal and fast energy groups. In the thermal group, a cavity appears in the center of the graph due to the presence of the source. Beyond the surface of the source, neutrons begin to moderate, reaching a peak thermal flux of approximately $2.4 \times 10^4 \text{ cm}^{-2} \text{ s}^{-1}$. The graph also illustrates the reflection effect on neutrons as they attempt to pass through the 20 cm water column along the reactor's sides. In the fast group, as expected, the peak occurs at the center, with a flux of around $1.6 \times 10^5 \text{ cm}^{-2} \text{ s}^{-1}$, rapidly decreasing as the distance from the center increases. Neutron interactions across the reactor geometry are clearly visible in Figure Fig. 5b. This radial cross-section allows us to make four observations: (1) the various peaks in thermal neutrons correspond to water-filled regions between the fuel rods, while the small peaks in fast neutrons represent areas containing fuel; (2) the double valleys in thermal flux are caused by capture reactions in the annular fuel; (3) the maximum flux in the lateral reflector zone is $1.23 \times 10^3 \text{ cm}^{-2} \text{ s}^{-1}$; and finally, (4) the peak thermal flux directly correlates with previous data, reaching $2.38 \times 10^4 \text{ cm}^{-2} \text{ s}^{-1}$.

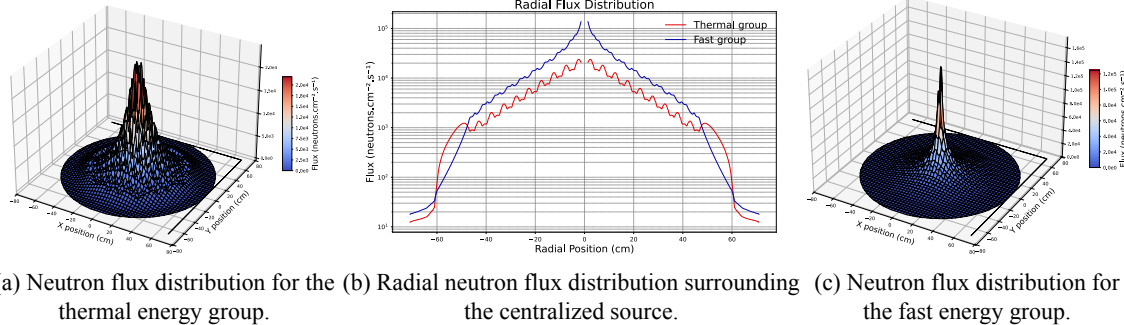


Figure 5. Spatial spectra of flux for two energy groups.

3.2. Irradiation Positions Analysis

As described previously, this section focuses on studying the neutron flux in two potential regions of interest for irradiation. With this in mind, Fig. 7 shows the energy spectra of the flux in both regions. For high-energy neutrons, above 0.1×10^6 eV, both regions exhibit similar behavior, differing only in the flux intensity. These high-energy neutron peaks reflect the discretization of the PuBe neutron source's emission spectrum, where larger peaks correspond to higher probabilities of neutron emission. Above the source, for neutrons below 4×10^2 eV, the energy group changes rapidly, while the flux remains almost constant. A similar pattern is observed for neutrons within the annular fuel. However, in the resonance range from 5.0 to 1.39×10^2 eV, neutron flux decreases by up to approximately 73%. In the thermal range, flux inside the annular fuel is lower due to radiative capture in uranium isotopes, with the peak being about 39% lower compared to above the source. To better evaluate neutron flux and the available space for efficient sample irradiation, a precise axial spatial spectrum was created, as shown in Fig. 6.

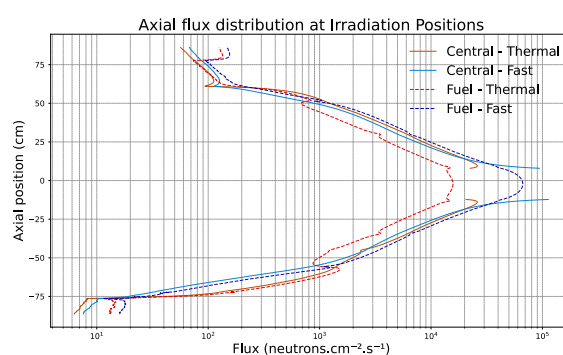


Figure 6. Axially divided spatial spectra of flux for two energy groups.

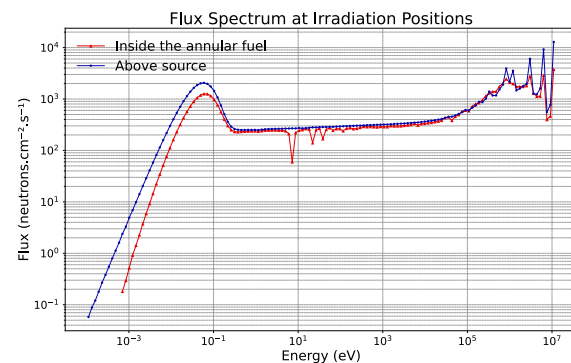


Figure 7. Energy spectra of flux in two regions: (1) inside the annular fuel closest to the center, and (2) above the source.

Inside annular fuel, the optimal region for irradiation applications is a cylinder with a diameter of 1.27 cm and a height of 22.74 cm. This area averages thermal and fast flux at $1.48 \times 10^4 \text{ cm}^{-2} \text{ s}^{-1}$ and $5.70 \times 10^4 \text{ cm}^{-2} \text{ s}^{-1}$, respectively. Above the source, a cylinder with a diameter of 3.32 cm



and a height of 4.60 cm is the most suitable for such applications. Here, the average neutron flux for thermal neutrons is around $2.48 \times 10^4 \text{ cm}^{-2} \text{ s}^{-1}$, while for fast neutrons it reaches $4.25 \times 10^4 \text{ cm}^{-2} \text{ s}^{-1}$.

4. CONCLUSION

This work conducted a neutronic analysis of the subcritical NC-9000, providing data on multiplication factors, flux distributions throughout the reactor, average fluxes at optimized irradiation positions, and effective doses in external regions of the reactor.

Although Monte Carlo simulations require high computational power, the simulation settings were more than sufficient to ensure accurate results. The lack of information regarding the original source used by ITA highlights the need to use a similar PuBe source.

In the first part of results, k_{eff} was determined to be 0.841897, closely aligning with the manufacturer's value of 0.842. This result differs significantly from the data reported by Motta [1], which are heavily affected by a large margin of error. However, this work shows good agreement with the simulation done by Vega-Carrillo, Garcia-Reyna, Marquez-Mata, *et al.* [8], differing only by 1.46%, likely due to variations in fuel density. Since the PuBe source is positioned within the nuclear system, the value of k_s exceeds k_{eff} , leading to a $\phi^* > 1$ and indicating an effective usage of the external neutron source. Taking this into account, ϕ^* equal 1.87 means that one neutron from source corresponds to 1.87 fission neutrons. Additionally, the neutron amplification factor (M) shows a net neutron increase by a factor of 11 in relation to the total emitted by the source. Thermal neutron flux reached a maximum of $2.4 \times 10^4 \text{ cm}^{-2} \text{ s}^{-1}$, while fast neutrons peaked at $1.6 \times 10^5 \text{ cm}^{-2} \text{ s}^{-1}$. Neutron moderation, capture in the annular fuel, and reflection from the lateral water layer were key factors affecting the flux distribution.

Second part is focused on studying the neutron flux in two regions of interest for irradiation. The energy spectrum analysis revealed that in resonance range between 5.0 and $1.39 \times 10^2 \text{ eV}$, a significant flux reduction of up to 73% was observed. Thermal neutron flux within the annular fuel was also reduced by approximately 39% due to radiative capture. Inside the annular fuel, the ideal irradiation zone was a cylinder with a diameter of 1.27 cm and a height of 22.74 cm, with thermal and fast fluxes averaging $1.48 \times 10^4 \text{ cm}^{-2} \text{ s}^{-1}$ and $5.70 \times 10^4 \text{ cm}^{-2} \text{ s}^{-1}$, respectively. Above the source, the most suitable region for irradiation was determined to be a cylinder with a diameter of 3.32 cm and a height of 4.60 cm, where thermal flux reached $2.48 \times 10^4 \text{ cm}^{-2} \text{ s}^{-1}$ and fast flux $4.25 \times 10^4 \text{ cm}^{-2} \text{ s}^{-1}$.

ACKNOWLEDGEMENTS

We would like to thank funding agency CAPES for indirect support provided to this work and CDTN/CNEM for providing information and facilitating visits to the disassembled parts of the subcritical reactor.

References

- [1] F. S. Motta, "Características do reator sub-crítico NC-9000", Master's thesis, Instituto Tecnológico de Aeronáutica - ITA, São José dos Campos, Brasil, 1970.
- [2] H. R. Vega-Carrillo, A. L. Aguilar-Dominguez, S. V. Bedenko, and G. F. García-Fernandez, "Computational spectrometry and dosimetry, of neutrons and γ rays, outside a subcritical nuclear reactor with water and polyethylene moderators", *Radiation Physics and Chemistry*, vol. 204, p. 110 719, 2023.



- [3] P. K. Romano, N. E. Horelik, B. R. Herman, A. G. Nelson, B. Forget, and K. Smith, “Openmc: A state-of-the-art monte carlo code for research and development”, *Annals of Nuclear Energy*, vol. 82, pp. 90–97, 2015.
- [4] KAERI. “Kaeri nuclear data center - tabelas de núclidos”. Accessed: September 5, 2024. (2024), [Online]. Available: <https://atom.kaeri.re.kr/>.
- [5] W. Huang, Y. Zhang, W. Dai, and R. Long, “Mechanical properties of 304 austenite stainless steel manufactured by laser metal deposition”, *Materials Science and Engineering: A*, vol. 758, pp. 60–70, 2019.
- [6] H. Vega-Carrillo, V. Hernández-Dávila, T. Rivera, and A. Sánchez, “Nuclear and dosimetric features of an isotopic neutron source”, *Radiation Physics and Chemistry*, vol. 95, pp. 122–124, 2014.
- [7] Y.-Q. Shi, Q.-F. Zhu, and H. Tao, “Review and research of the neutron source multiplication method in nuclear critical safety”, *Nuclear technology*, vol. 149, no. 1, pp. 122–127, 2005.
- [8] H. R. Vega-Carrillo, M. G. Garcia-Reyna, C. A. Marquez-Mata, J. Vazquez-Bañuelos, G. E. Campillo-Rivera, and S. V. Bedenko, “Effect of changing the neutron moderator in a thermal subcritical nuclear reactor”, *Applied Radiation and Isotopes*, vol. 188, p. 110395, 2022.